EUROPEAN ORGANIZATION FOR NUCLEAR RESEARCH

L3 Note 2570
June 30, 2000

Total Cross Section in $\gamma\gamma$ Collisions at LEP

The L3 Collaboration

Abstract

The reaction $e^+e^- \rightarrow e^+e^-\gamma^*\gamma^* \rightarrow e^+e^-$ *hadrons* is analysed for quasi-real photons using data collected by the L3 detector during the LEP high energy runs from $\sqrt{s} = 189$ GeV to 202 GeV. Results on the total cross sections $\sigma(e^+e^- \rightarrow e^+e^-$ *hadrons*) and $\sigma(\gamma\gamma \rightarrow$ *hadrons*) are given in the interval 5 GeV $\leq W_{\gamma\gamma} \leq$ 145 GeV. The centre-of-mass energy dependence of the two-photon cross section is described by the universal Regge parametrisation. We observe a steeper rise with energy as compared to hadron-hadron cross sections. The data are also compared to the expectation of different theoretical models.

Submitted to the
XXXth International Conference on High Energy Physics
Osaka, Japan, July 27 - August 2, 2000.

1 Introduction

At high energies the two-photon process $e^+e^- \to e^+e^-\gamma^*\gamma^* \to e^+e^-$ *hadrons* is a copious source of hadron production. In this reaction most of the initial energy is taken by the scattered electrons and positrons. As their scattering angle is close to the beam they often go undetected. The hadron system has typically a low mass compared to $\sqrt{s}$. A large fraction of the hadrons escape detection, due to the large diffractive cross section and to the Lorentz boost of the $\gamma\gamma$ system. For these events, the measured visible mass $W_{\rm vis}$ is smaller than the two photon effective mass $W_{\gamma\gamma}$. For high values of $\sqrt{s}$ the $W_{\rm vis}$ spectrum of two-photon processes is well separated from that of the e^+e^-annihilation processes.

In this paper we analyse only data where the scattered electrons are not detected (anti-tagged events). New results on total cross section $\sigma($ $e^+e^- \to e^+e^-$*hadrons*) are presented for the e^+e^-centre of mass energies $\sqrt{s}= 189 - 202$ GeV. The two-photon cross section $\sigma(\gamma\gamma \to$ *hadrons*) is then derived in the interval $5 \leq W_{\gamma\gamma} \leq 145$ GeV. The analysis of the data taken at $\sqrt{s}= 130 - 161$ GeV [1] is superceeded by the present analysis which covers a wider mass interval and has twenty times more statistics.

After the description of the event selection and the comparison of the data with existing Monte Carlo models, we discuss Regge fits to the data and make a comparison with QCD models .

2 Event selection

Data have been collected with the L3 detector at $\sqrt{s}= 189$ GeV with a total integrated luminosity of 171.8 pb^{-1} during 1998 and at $\sqrt{s}= 192$, 196, 200, 202 GeV with a total integrated luminosity of 220.8 pb^{-1} during 1999.

A detailed description of each subsystem of the L3 detector and its performance is given in [2] and [3]. The analysis described in this paper is mainly based on the central tracking system, the high resolution electromagnetic calorimeter and the hadron calorimeter. Particles scattered at small angles are measured by the luminosity monitors on each side of the detector, covering a polar angle range between 33 and 64 mrad.

The events used in this analysis are collected predominantly by the track triggers [4]

Hadronic two-photon events are selected by the following criteria :

- At least six particles must be detected (Fig.1a,b). A particle can be a track, a photon or an hadronic cluster in the hadron calorimeter or in the luminosity monitor. A track must have a transverse momentum $p_t > 100$ MeV, at least 12 wire hits and a distance of closest approach to the nominal vertex less than 10 mm in the transverse plane A photon candidate is a cluster in the electromagnetic calorimeter, with no nearby track within 200 mrad and the associated energy in the hadron calorimeter smaller than 20% of the electromagnetic energy. Clusters in the hadron calorimeter, without any track in a 300 mrad cone and with an energy greater than 20% of the electromagnetic energy are considered as pions, since they are mainly outside the track chamber detection region. Clusters in the luminosity monitor with energy less than 30 GeV are considered as pions if their energy is below 5 GeV and as photons above 5 GeV.

- The total energy in the electromagnetic calorimeter is required to be greater than 500 MeV in order to suppress beam-gas and beam-wall backgrounds and smaller than 50

GeV, to exclude events of the type $e^+e^- \to \gamma(Z \to q\bar{q})$. The total energy deposited in the calorimeters must be smaller than 40 % of the centre of mass energy, to exclude annihilation events (Fig.1c).

- An anti-tag condition is imposed which excludes events with clusters having energy greater than 30 GeV in the luminosity monitor, in a fiducial region of 33−64 mrad (Fig.1d). The Q^2 value of the selected events is thus less than 8 GeV^2, its average value being $< Q^2 >\sim 1.5\ 10^{-2}$ GeV^2

After selection, the background from beam-gas and beam-wall interactions is found to be negligible. The visible effective mass of the event is calculated from the four-momentum vectors of the measured particles:

$$W_{\rm vis}^2 = (\sum_i E_i)^2 - (\sum_i \vec{p}_i)^2$$

The analysis is limited to events with $W_{\rm vis} \geq 5$ GeV. Almost 2 million events are selected, 781511 at $\sqrt{s}= 189$ GeV and 1027939 at $\sqrt{s}= 189 - 202$ GeV. The observed cross-section is $\sim$ 4.6 nb, stable during the data taking period.

The $\gamma\gamma \to$ *hadrons* processes are simulated with the PHOJET [1)] [5] and PYTHIA [2)] [6] event generators. For the annihilation processes $e^+e^- \to$ *hadrons*(γ), ZZ(γ), Zee(γ), We$\nu(\gamma)$ we have simulated events with PYTHIA [6]; we have used KORALZ [7] for $e^+e^- \to \tau^+\tau^-(\gamma)$ and KORALW [8] for $e^+e^- \to W^+W^-$. For the $e^+e^- \to e^+e^-\tau^+\tau^-$ channel the generator DIAG36 [9] was used. The events were simulated in the L3 detector using GEANT [10] and GEISHA [11] programs and passed through the same reconstruction program as the data.

Comparison of the data with Monte Carlo predictions are shown in Fig.1 and Fig.2. The energy distribution in the luminosity monitor (Fig.1b) shows a good agreement for the low energy clusters, which are used in the $W_{\rm vis}$ calculations. When the scattered electron or positron reaches the detector, the agreement is maintained with the PHOJET Monte Carlo, while these configurations are missing in PYTHIA because of a cutoff $Q^2 \leq m_\rho^2$ applied to the two-photon luminosity function in the generation of the events. Otherwise generally good agreement between data and Monte Carlo is observed.

The background is below 1% at low masses, dominated by the two-photon τ production. It increases at high masses, due mainly to annihilation processes and reaches a maximum of $\simeq$ 15% at 130 GeV. In Fig.3a the $W_{\rm vis}$ spectrum is shown for the full data sample.

The trigger inefficiency is studied separately for each data sample by comparing the response of the track trigger to the response of the calorimetric energy triggers. The higher level triggers are studied with prescaled rejected events. The trigger efficiency is mass dependent varying from $\simeq$ 80 % at $W_{\rm vis}$=5 GeV to $\simeq$ 94 % for $W_{\rm vis} >$ 80 GeV.

3 Measurement of cross sections

3.1 Unfolding and efficiency

From the observed distribution of the visible effective mass, $W_{\rm vis}$, the true hadron mass $W_{\gamma\gamma}$ distribution must be extracted. The number of observed events are then corrected for the efficiency and acceptance of the detector.

[1)] PHOJET version1.05c

[2)] PYTHIA version 5.718 and JETSET version 7.408

The measured W_{vis} spectrum is weakly correlated to the total centre of mass energy of the $\gamma\gamma$ system because a large part of the produced particles go undetected in the forward and backward regions. In order to obtain the $\mathrm{W}_{\gamma\gamma}$ distribution, subdivided in 8 i-intervals, from the W_{vis} spectrum, subdivided in 16 j-intervals, the following unfolding relation is used:

$$N(W_{\gamma\gamma}(i)) = \sum_{j=1}^{16} A_{ij} N(W_{\mathrm{vis}}(j)) \tag{1}$$

The matrix A_{ij} is constructed by considering for each Monte Carlo event the measured W_{vis} and its generated $W_{\gamma\gamma}$ value as follows [12]:

$$A_{ij} = \frac{P(W_{\mathrm{vis}}(j)|W_{\gamma\gamma}(i))P(W_{\gamma\gamma}(i))}{\sum_{l=1}^{8} P(W_{\mathrm{vis}}(j)|W_{\gamma\gamma}(l))P(W_{\gamma\gamma}(l))} \tag{2}$$

where $P(W_{\mathrm{vis}}|W_{\gamma\gamma})$ is the likelihood of observing the measured W_{vis} given a generated $W_{\gamma\gamma}$value and $P(W_{\gamma\gamma})$ is the initially generated $W_{\gamma\gamma}$ distribution after acceptance and efficiency cuts.

The result of the unfolding is somewhat dependent on the Monte Carlo used to construct the matrix A_{ij} (Fig.3b). Data unfolded with PYTHIA are up to 20% higher than if unfolded with PHOJET. After unfolding, the events are corrected for detector acceptance and efficiency using the ratio between selected and generated events in each $W_{\gamma\gamma}$ interval (Fig.3c). This includes geometrical effects as well as inefficiencies of the detector and of the analysis cuts. The low acceptance below $W_{\gamma\gamma}$= 30 GeV is due to the W_{vis} cutoff of 5 GeV. For $W_{\gamma\gamma}>$ 30 GeV, the acceptance is rather constant. There is a systematic difference of $\simeq$ 10% between the efficiencies given by the two Monte Carlo models, this may be attributed to a different modeling of the diffractive interactions which are not easily seen in the detector.

Although the data are better reproduced by PHOJET, the analysis of specific hadronic channels, the diffractive ρ [13] and the inclusive charm [14] production, show some inadequacy of the PHOJET simulation. For this reason and in order to use the maximum Monte Carlo statistics for unfolding, we use in this analysis both Monte Carlos, with equal statistics, to unfold and correct the data [3)].

3.2 Cross sections and systematic errors

From the number of events, corrected with the Monte Carlo in each $W_{\gamma\gamma}$ bin, and the integrated $\mathrm{e^+e^-}$ luminosity, the cross section $d\sigma(\mathrm{e^+e^-} \rightarrow \mathrm{e^+e^-} hadrons)$ is measured. The differential cross section $\mathrm{d}\sigma/\mathrm{d}W_{\gamma\gamma}$ is shown in Fig.3d together with our measurements at lower LEP collision energy. The fast decrease of the cross section as a function of $W_{\gamma\gamma}$ is due to the two photon luminosity function, $\mathcal{L}_{\gamma\gamma}$, which depends on $\tau = W_{\gamma\gamma}^2/s$. The measurements for $\sqrt{s} = 189$ GeV and for $\sqrt{s} = 196 - 202$ GeV are given in Table 1.

To extract the total cross section of two real photons the photon flux $\mathcal{L}_{\gamma\gamma}$ [15] must be calculated and the hadronic two-photon processes must be extrapolated to $\mathrm{Q}^2 = 0$. This is done by considering the dominant transverse photon (T) interaction as well as the small scalar photon (S) contribution [16] :

$$d\sigma(\mathrm{e^+e^-} \rightarrow \mathrm{e^+e^-} hadrons)/d\tau = \int \frac{d(Q_1^2)}{Q_1^2} \frac{d(Q_2^2)}{Q_2^2} \sum_{a,b=T,S} \mathcal{L}_{ab} \sigma_{ab}(W_{\gamma\gamma}, Q_1^2, Q_2^2). \tag{3}$$

[3)] For the previous results, Ref. [1] and in conference papers, our preference was given to PHOJET. The cross section values were therefore below the values presented here, since the cross sections corrected with PHOJET are systematically lower than the ones corrected with PYTHIA.

The $W_{\gamma\gamma}$ and Q^2 dependencies of the cross section can be factorized for $Q^2 << W_{\gamma\gamma}^2$:

$$\sigma_{a,b}(W_{\gamma\gamma}, Q_1^2, Q_2^2) = F_a(Q_1^2)F_b(Q_2^2)\sigma_{\gamma\gamma}(W_{\gamma\gamma}, 0., 0.) \tag{4}$$

For each $W_{\gamma\gamma}$ bin a numerical integration is performed over the bin width and over the unmeasured Q^2 of the scattered electron and positron. Many forms have been proposed for the $F(Q^2)$ form factors. A model [17], which adds a continuum contribution to a simple vector-meson dominance contribution, has been chosen for the central value calculation:

$$\begin{aligned} F_T(Q^2) &= \sum_V r_V \left(\frac{m_V^2}{m_V^2 + Q^2}\right)^2 + r_c \frac{m_0^2}{m_0^2 + Q^2} \\ F_S(Q^2) &= \sum_V \xi \frac{Q^2}{m_V^2} r_V \left(\frac{m_V^2}{m_V^2 + Q^2}\right)^2 \end{aligned}$$

where V = ρ, ω, ϕ, ξ= 1/4, r_ρ=0.65, r_ω=0.08, r_ϕ=0.05 and $r_c = 1 - r_\rho - r_\omega - r_\phi$. Depending on the form factors used, this calculation may vary by $\pm 5\%$ [16].

The systematic errors are evaluated for each $W_{\gamma\gamma}$ bin (Table 2):

- Uncertainties on the trigger rejections are evaluated by variying the trigger efficiency inside the accuracy of its determination ($\simeq$ 10 %)
- Uncertainties on the energy scale of the calorimeters and of the annihilation background are evaluated by varying the energy cut by $\pm 0.1\sqrt{s}$.
- Uncertainties on the energy scale of the small angle calorimeter are evaluated by varying the gain by a factor two, they are found to be negligible.
- Uncertainties on the tag condition are evaluated by changing the anti-tag cut from 30 to 50 GeV.
- Uncertainties on the particle multiplicity are evaluated by displacing the cut on the minimum number of particles from six to four and eight particles.
- Uncertainties related to the unfolding are evaluated by using different sets of Monte Carlo events. They affect only the high masses, where the Monte Carlo statistics is poor.

The mass dependent statistical and systematic errors are added in quadrature in each $W_{\gamma\gamma}$ bin in the figures and for the Regge fit. The uncertainty related to the Monte Carlo model, evaluated by repeating the analysis with PYTHIA and PHOJET separately, is the largest individual contribution almost in all bins and is considered separately.

The $\gamma\gamma \rightarrow$ *hadrons* cross sections at $\sqrt{s}$= 189 GeV and $\sqrt{s}$= 196-202 GeV are compared in Fig.4a. The two sets of data are compatible within the experimental systematic errors, the combined value is given in Table 4 with the statistical errors obtained from unfolding, experimental systematics and model systematics. The model systematics takes into account the different result from PYTHIA and PHOJET (Fig.4b) and the uncertainty on the form of the luminosity function.

3.3 Regge parametrisation

The total hadronic cross sections show a characteristic steep decrease in the region of low centre of mass energy followed by a slow rise at high energies. From Regge theory [18] this behaviour is understood as the consequence of the exchange of Regge trajectories, $\alpha(t)$, in the t-channel. The total cross section takes the form $\sigma_{\rm tot} \propto s^{(\alpha(0)-1)}$. The low energy region is sensitive to Reggeon exchange (R = ρ, ω, f, a ..), $\alpha_R(0) \simeq 0.5$. At high energies the Pomeron exchange dominates, $\alpha_P(0) \simeq 1$. A.Donnachie and P.V. Landshoff [19] showed that a parametrisation of the form

$$\sigma_{\rm tot} = A\, s^{\epsilon} + B\, s^{-\eta} \tag{5}$$

can account for the energy behaviour of all hadronic and photoproduction total cross sections, the powers of s being universal. This is confirmed by the recent compilation of the total cross section data [20] where a fit of Eq.5 for all hadron total cross sections gives a result compatible with a universal value of $\epsilon = 0.095 \pm 0.002$ and $\eta = 0.34 \pm 0.02$. The coefficients A and B are process and Q^2 dependent. If photons behave predominantly like hadrons, this expression may also be valid for the two-photon total hadronic cross section. The data are fitted to Eq.5 with the parameters ϵ and η fixed to the universal value (Table 3). The fit, dashed line in Fig.4b, does not represent well the $\sigma_{\gamma\gamma}$ energy dependence. Taking into account statistical and experimental systematic errors and the correlation matrix between the measured points, we obtain $\chi^2 = 110$ for 12 [4)] degrees of freedom. We therefore try a fit with A, B and ϵ as free parameters (Fig.4 and Table 3), we obtain :

$$\epsilon = 0.250 \pm 0.016 \qquad CL = 30\%$$

This value is more than a factor two higher than the universal value, independent on the Monte Carlo model used to correct the data. The fitted value of ϵ is strongly correlated to the Reggeon component. To avoid this correlation we fit only the Pomeron exchange for sufficiently high $W_{\gamma\gamma}$ values. The results, using a different initial value of $W_{\gamma\gamma}$, are listed in Table 3. The value of ϵ increases by increasing the lower mass cutoff, thus indicating a somewhat variable slope due to the inset of QCD phenomena.

3.4 Models for $\gamma\gamma$ total cross sections

In a pure Regge theory the Pomeron intercept is 1 and the total cross sections must be constant. When the rise of the proton proton total cross section was first observed, it was proposed [21] that this rise was due to an increase of the number of hard interactions among the constituents of the hadrons. The lack of unitarity of the original models was cured by the introduction of eikonalized mini-jet models.

The calculation of the mini-jet model of R.M.Godbole and G.Pancheri [22], rescaled by a factor 1.1, is shown in Fig.5a as a continous line. This model ascribes to QCD the task of calculating the average number of semi-hard collisions n(b,s), which are a function of the impact parameter b and of the centre of mass energy s. The collisions are assumed to be independent of each other at a fixed value of the impact parameter b and to have a Poisson type distribution around the average value. The calculation depends on the choice of the lowest transverse momentum used in the hard jet cross section $\sigma_{jet} = \int_{p_{tmin}} \frac{d\sigma}{dp_t^2} dp_t^2$ and on the parameter k_0 which defines the b-distribution of partons in the photon. In Fig.5a the parameters which fit best the photoproduction data are used p_{tmin} =2 GeV and k_0 =0.66 GeV, together with

[4)] The two set of data are fitted separately the GRV parton density function. The predictions are multiplied by a scale factor 1.1, which implies a somewhat lower value of k_0.

Recently models with two Pomerons have been proposed [23] to explain the fast energy increase of deep inelastic scattering J/ψ photoproduction. In these schemes, corresponding to a colour-dipole picture for the high energy scattering amplitude, there are two trajectories carrying the vacuum quantum numbers with different fixed intercepts and with residues dependent on Q^2. The "soft Pomeron" has intercept $\alpha_{soft}(0) \sim 1.08$ and the "hard Pomeron" $\alpha_{hard}(0) \sim 1.4$. Because of the $\mathrm{q\bar{q}}$ component in the photon wave-function the hard Pomeron contributes to the two-photon cross-section also at $Q^2 = 0$. This model predicts a more rapid energy dependence for $\sigma_{\gamma\gamma}$ than for a normal hadron, the value of ϵ is evaluated to be $\sim 0.14-0.15$ in our measured energy range. The absolute value of $\sigma_{\gamma\gamma}$ depends on the quark mass used, the cross-section value being smaller if the quark mass is higher.

The ultimate description of high energy photon interactions should be derivable from the QCD Lagrangian. At the present level of theoretical understanding a perturbative QCD contribution is added to the non perturbative diffractive phenomenology. One can represent the photon as the superposition of the *bare* photon and the *hadronic* photon :

$$\mid \gamma >= \sqrt{Z_3} \mid \gamma_{bare} > + \frac{e}{f_{\mathrm{q\bar{q}}}} \mid \mathrm{q\bar{q}} > + \frac{e}{f_{\mathrm{q\bar{q}^*}}} \mid \mathrm{q\bar{q}}^* > \tag{6}$$

where

$$Z_3 = 1 - (\frac{e}{f_{\mathrm{q\bar{q}}}})^2 - (\frac{e}{f_{\mathrm{q\bar{q}^*}}})^2 \tag{7}$$

The *bare* photon interacts via *direct* processes, i.e. the photon participate directly into the scattering processes as in the QED interaction $\gamma\gamma\to \mathrm{q\bar{q}}$. For the *hadronic* component it is assumed that the photon fluctuates into a $\mathrm{q\bar{q}}$ pair which interacts hadronically. Due to the quantum numbers of the photon, it is expected that the $\mathrm{q\bar{q}}$ pairs form particles with small masses like ρ, ω, ϕ vector mesons (VDM). The hadronic interactions are divided into hard ($\mathrm{q\bar{q}}^*$) and soft interactions by a transverse momentum cutoff p_t^{cut}. The subprocesses involving transverse momenta greater than this scale can be calculated by lowest order perturbative QCD. The $\gamma\gamma$ cross section is therefore composed by a "soft VDM" interaction, which can be described by hadronic phenomenology, like the Regge poles, a point like two-photon reaction, $\gamma\gamma\to \mathrm{q\bar{q}}$, which is exactly calculable in QED (direct or QPM component) and an "hard component" (anomalous or QCD component) which implies the knowledge of the quark and gluon structure in the photon. In order to describe the data the models have to include

- a consistent transition between low p_t and high p_t events
- a description of elastic and diffractive reactions like $\gamma\gamma\to$VV
- a description of the structure of the photon and of the primordial k_T distribution of the partons inside the photon
- a unitarization scheme for the jet cross sections.

The model of G.A. Schuler and T. Sjöstrand [24] aims at a smooth superposition of hadron-like and point-like photon interactions. Following their discussion, one sees that the fluctuation of both photons into vector mesons is not sufficient to describe the data (lower, dashed−line in Fig.5b). Adding the point-like interactions of at least one photon, the cross section increases to values comparable to our data points. The maximum QCD contribution, allowed by unitarity, is indicated by the dotted−line.

The cross sections predicted by R.Engel and J.Ranft [5], rescaled by a factor 1.1, (dashed−line in Fig.5a) are in good agreement with the data. In their model γp and pp data are used to fix the couplings of the Pomeron and of the Reggeon to the q$\bar{\mathrm{q}}$ fluctuation of the photon. The cross sections are then calculated in the framework of a Dual Parton Model, with the unitarization constraint. Since there is a correlation between the VDM couplings and the Pomeron parameters, the predictions have an accuracy of $\pm 10\%$ [5].

Many models where recently compared to the L3 and OPAL [25] measurements. Often they constrain the two-photon cross section with the measurements of proton-proton and photoproduction total cross sections, by assuming factorization for the Pomeron residue: $\sigma_{\gamma\gamma} \approx \sigma^2_{\gamma\mathrm{p}}/\sigma_{\mathrm{pp}}$ [26]. In general these models give an energy dependence of the cross section similar to the universal fit, some examples [27], [28], [29] are shown in Fig.5c) and d). As it can be seen in Fig.5 d), our result is in very good agreement with the OPAL measurement [25], this is true also if the two experiments unfold their data with only PYTHIA or PHOJET models.

4 Conclusions

The cross section $\sigma(\ \mathrm{e}^+\mathrm{e}^- \rightarrow \mathrm{e}^+\mathrm{e}^- hadrons)$ for untagged events is measured at LEP, with the L3 detector, at 189 GeV $\leq \sqrt{s} \leq$ 202 GeV, in the interval 5 GeV$\leq W_{\gamma\gamma} \leq$ 145 GeV. The real photon total cross section $\sigma(\gamma\gamma \rightarrow hadrons)$, derived from the data, increases as a function of $W_{\gamma\gamma}$, faster than expected from the universal fit of hadron-hadron total cross-sections. The observed energy dependence can be reproduced by introducing a hard Pomeron component or by QCD models which include an important contribution of the hard scattering of the partons inside the photon.

Acknowledgements

We express our gratitude to the CERN accelerator divisions for the excellent performance of the LEP machine. We acknowledge with appreciation the effort of all engineers, technicians and support staff who have participated in the construction and maintenance of this experiment.

References

[1] L3 Coll., M. Acciari et al.,Phys. Lett. **B 408** (1997) 450.

[2] L3 Coll.,B.Adeva et al., Nucl. Inst. Meth. **A 289** (1990) 35.

[3] M. Acciarri et al., Nucl. Inst. Meth. **A 351** (1994) 300.

[4] P.Béné et al., Nucl. Inst. Meth. **A 306** (1991) 150;
D. Haas et al., Nucl. Inst. Meth. **A 420** (1999) 101.

[5] R. Engel, Z. Phys. **C 66** (1995) 203 ;
R. Engel and J. Ranft, Phys. Rev. **D 54** (1996) 4246;
And R. Engel private communication.

[6] T. Sjöstrand, Comput. Phys. Commun. **82** (1994) 74.

[7] S.Jadach,B.F.L.Ward and Z.Was, Comput. Phys. Commun. **79** (1994) 503.

[8] M.Skrzypek, S.Jadach,W. Placzek, and Z.Was, Comput. Phys. Commun. **94** (1996) 216.

[9] F.A.Berends,P.H.Daverfeldt and R.Kleiss, Nucl. Phys. **B 253** (1985) 441.

[10] R.Brun et al., GEANT 3.15 preprint CERN DD/EE/84-1 (Revised 1987).

[11] H.Fesefeldt, RWTH Aachen report PITHA 85/2 (1985).

[12] G. D'Agostini, Nucl. Inst. Meth. **A 362** (1995) 487.

[13] Á. Csilling, Diffractive Vector Meson Production in Photon-Photon Interactions, Ph.D. thesis, Eötvös Univerity, Budapest, 1999, L3 internal note 2487.

[14] L3 Collab., M. Acciarri et al., Phys. Lett. B 453 (1999) 83; and Phys. Lett. B 467 (1999) 137.

[15] V.M. Budnev, I.F. Ginzburg, G.V. Meledin and V.G. Serbo, Phys.Rep. **C 15** (1974) 181.

[16] G.A. Schuler, Improving the equivalent-photon approximation in electron-positron collisions, hep-ph/9610406, CERN-TH/96-297.
We wish to thank the author for providing us with the numerical integration program of the luminosity function.

[17] J.J. Sakurai and D. Schildknecht, Phys. Lett. **B40** (1972) 121.

[18] P.D.B. Collins, Introduction to Regge theory (Cambridge U.P.,Cambridge, 1977)

[19] A.Donnachie and P.V. Landshoff, Phys. Lett. **B 296** (1992) 227.

[20] Review of Particle Physics, Eur.Phys.J. **C3** (1998) 1.

[21] D.Cline,F.Halzen and J.Luthe, Phys. Rev. Lett. **31** (1973) 491.

[22] R.M.Godbole and G.Pancheri, hep-ph/9903331 (1999);
A. Corsetti, R.M.Godbole and G.Pancheri, Phys. Lett. **B435** (1998) 441.

[23] A. Donnachie, H.G. Dosch and M. Rueter hep-ph/9810206 (1999).

[24] G.A. Schuler and T. Sjöstrand, Nucl. Phys. **B 407** (1993) 539 ;
G.A. Schuler and T. Sjöstrand, Z. Phys. **C 73** (1997) 677.

[25] OPAL Coll.,K. Ackerstaff et al., CERN EP/99-076 to be published in Eur. Phys. J C.

[26] V.N.Gribov and I.Ya.Pomeranchuk, Phys. Rev. Lett. **8** (1962) 343.
S.J.Brodsky, J.Phys.Suppl. (Paris) **35** (1974) C2-69.
K.V.L.Sarma and V. Singh , Phys. Lett. bf B 101 (1981) 201.

[27] B. Badelek, J. Kwiecinski and A.M. Stasto hep-ph/9903248 (1999) and hep-ph/0001161 (2000)

[28] P. Desgrolard, M. Giffon, E. Martynov and E. Predazzi hep-ph/9811393 (1999) to be published in Eur. Phys. J C.

[29] C. Bourrely, J. Soffer, T.T. Wu, CERN-TH/99-76.

$\Delta W_{\gamma\gamma}$	189 GeV		192 − 202 GeV		all data
(GeV)	$d\sigma_{e^+e^-}$(nb)	$\sigma_{\gamma\gamma}$(nb)	$d\sigma_{e^+e^-}$(nb)	$\sigma_{\gamma\gamma}$(nb)	$\sigma_{\gamma\gamma}$(nb)
5-9	5.01	402.3	5.06	395.9	399.1 ±0.5±30.±32.
9-17	3.35	367.8	3.46	368.1	367.9 ±0.4±19.±18.
17-31	1.88	357.1	1.97	359.7	358.4 ±0.5±12.±25.
31-47	0.810	378.2	0.862	381.2	379.7 ±0.8±8±35.
47-65	0.419	414.8	0.456	420.1	417.5 ±1.2±8.±46.
65-105	0.350	477.2	0.388	480.9	479.1 ±1.5±11.±62.
105-145	0.094	580.2	0.112	589.1	584.7 ±3.3±35.±109.

Table 1: The measured $d\sigma(\,e^+e^- \rightarrow e^+e^- hadrons)$ and $\sigma(\gamma\gamma \rightarrow hadrons)$ cross sections as a function of the $\gamma\gamma$ centre of mass energy for the two sets of data. The cross section $\sigma(\gamma\gamma \rightarrow hadrons)$ is also given for the combined data sample. The statistical errors, obtained after unfolding, the experimental systematic errors and the model error including Monte Carlo and photon luminosity uncertainties are given only for the combined data.

$W_{\gamma\gamma}$ GeV	Trigger %	energy cut %	antitag %	particles %	experimental %	model %
5-9	0.9	0.1	< 0.1	7.4	7.5	6.2
9-17	0.9	0.1	< 0.1	5.0	5.1	0.4
17-31	0.7	0.1	< 0.1	3.2	3.3	5.0
31-47	0.6	0.2	0.2	2.0	2.1	8.0
47-65	0.5	0.2	0.1	1.7	1.8	10.2
65-105	0.4	0.2	1.1	1.7	2.4	12.2
105-145	0.4	0.3	3.0	1.3	6.0	18.0

Table 2: Evaluation of systematic uncertainties. All values are per-cent uncertainties on the cross-section. A 5 % uncertainty on the photon luminosity function must also be added to the model uncertainty for the cross sections $\sigma(\gamma\gamma \rightarrow hadrons)$

fit	$W_{\gamma\gamma}$ interval	A	B	η fixed	ϵ	χ^2/d.o.f.	C.L.
	5-145 GeV	47. ± 7.	1048.± 97.	0.34	0.250 ± 0.016	13/11	0.30
	5-145 GeV	184. ± 3.	269.± 78.	0.34	0.095 fixed	110/12	
PHOJET	5-145 GeV	40. ± 9.	1173.± 100.	0.34	0.253 ± 0.025	15/11	0.17
PYTHIA	5-145 GeV	45. ± 8.	997.± 99.	0.34	0.271 ± 0.020	8/11	0.74
	17-145 GeV	206±7	0.	—	0.089±0.005	87/8	
	31-145 GeV	133±8	0.	—	0.144±0.008	14/6	0.03
	47-145 GeV	96±11	0.	—	0.183±0.014	3.2/4	0.53

Table 3: Fit to the total cross section of the form [19] $\sigma_{\gamma\gamma}= A\,s^{\epsilon} + B\,s^{-\eta}$, where $s = W^2_{\gamma\gamma}$. The data sets at $\sqrt{s}$=189 GeV and $\sqrt{s}$=192-202 GeVare separately included in the fit. The statistical and experimental errors and the correlation matrix between the data points are used. The fitted parameters are strongly correlated. The second set of fits evaluates only the increase of $\sigma_{\gamma\gamma}$ with s, i.e. the Pomeron part of the fit. PHOJET and PYTHIA indicate that only this Monte Carlo is used to unfold the data.

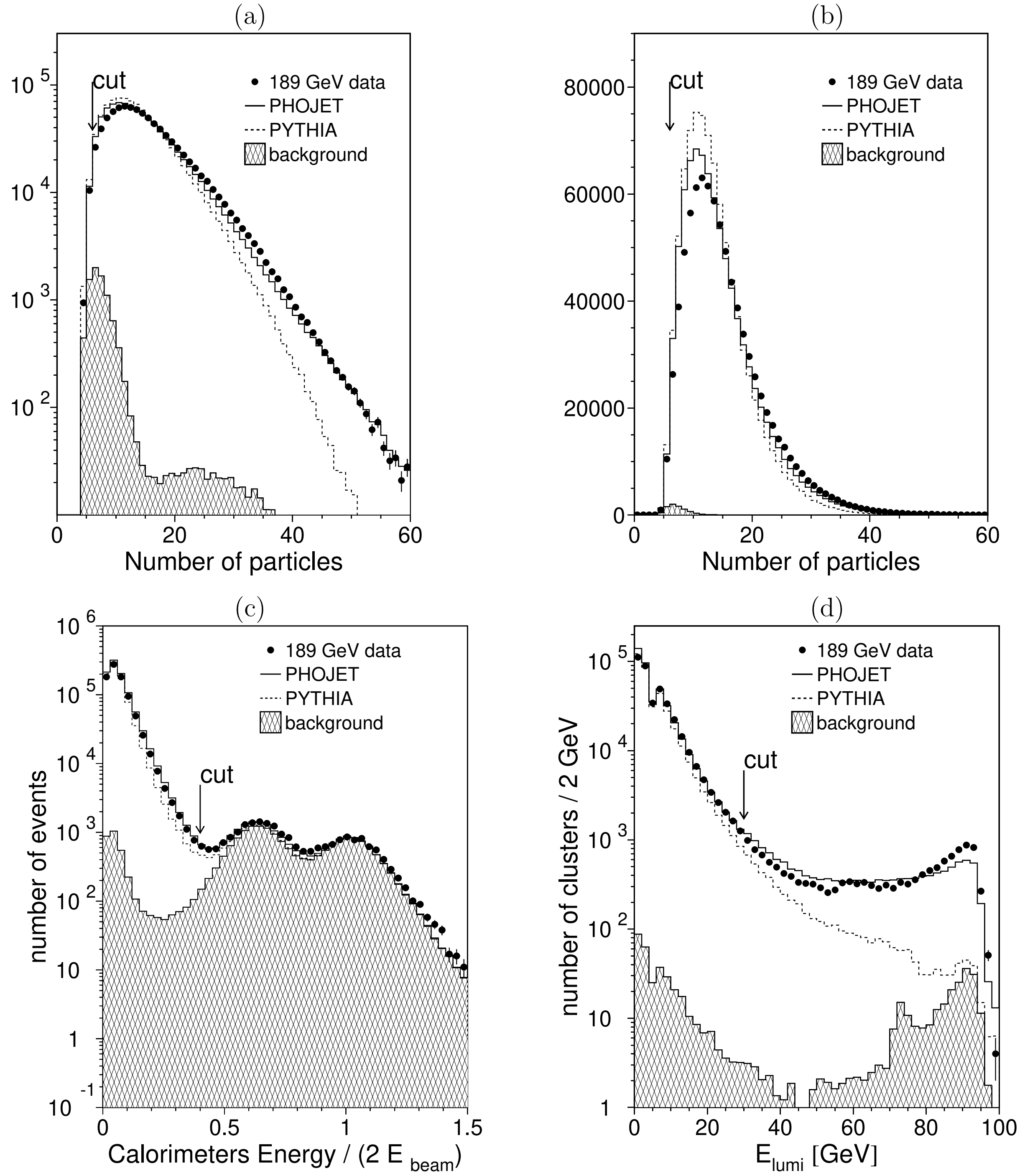

Figure 1: Distribution of the quantities used for the event selection. a)Number of particles in logarithmic scale b)Number of particles linear scale. c) Energy in the electromagnetic and hadronic calorimeters normalised to the centre-of-mass energy d) Energy in the luminosity monitor calorimeter, the cut at 30 GeV separates the untagged from the tagged sample. The data are compared with Monte Carlo predictions. The backgrounds due to e^+e^-annihilation and $e^+e^- \rightarrow e^+e^-\tau\tau$ are indicated as a shaded area.

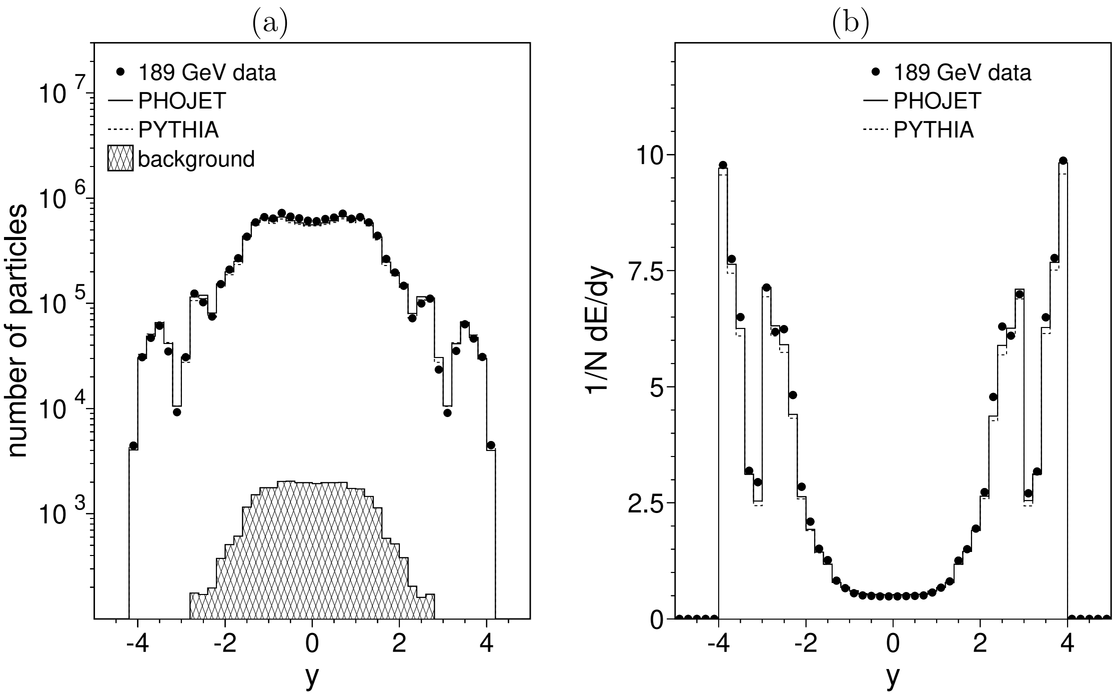

Figure 2: Comparison of some experimental distribution to PHOJET and PYTHIA expectations: a) The rapidity y distribution of the measured particles (pions or photons) b) Average energy of the measured particles as a function of y.

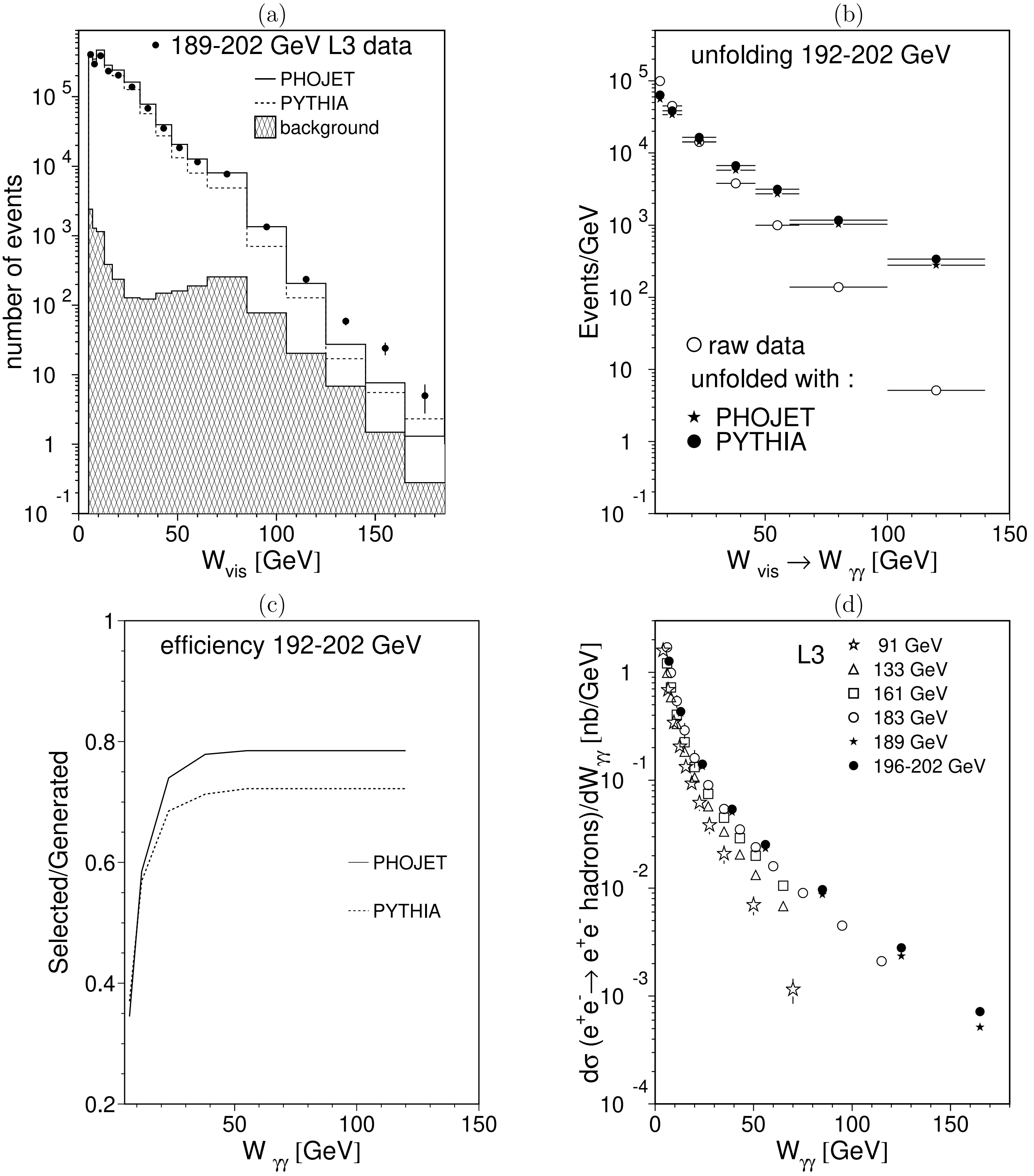

Figure 3: a) The measured hadronic mass W_{vis}. The backgrounds due to e^+e^-annihilation and $e^+e^- \to e^+e^-\tau\tau$ are indicated as a shaded area. b) The unfolding of the data from W_{vis} to $W_{\gamma\gamma}$. c) Ratio of selected over generated events as a function of the two-photon mass, as calculated by the two generators PHOJET and PYTHIA. d) The cross section $d\sigma(\ e^+e^- \to e^+e^- hadrons)/dW_{\gamma\gamma}$ measured at various beam energies, 91 GeV$\leq \sqrt{s} \leq$ 202 GeV. The statistical and systematic errors are added in quadrature.

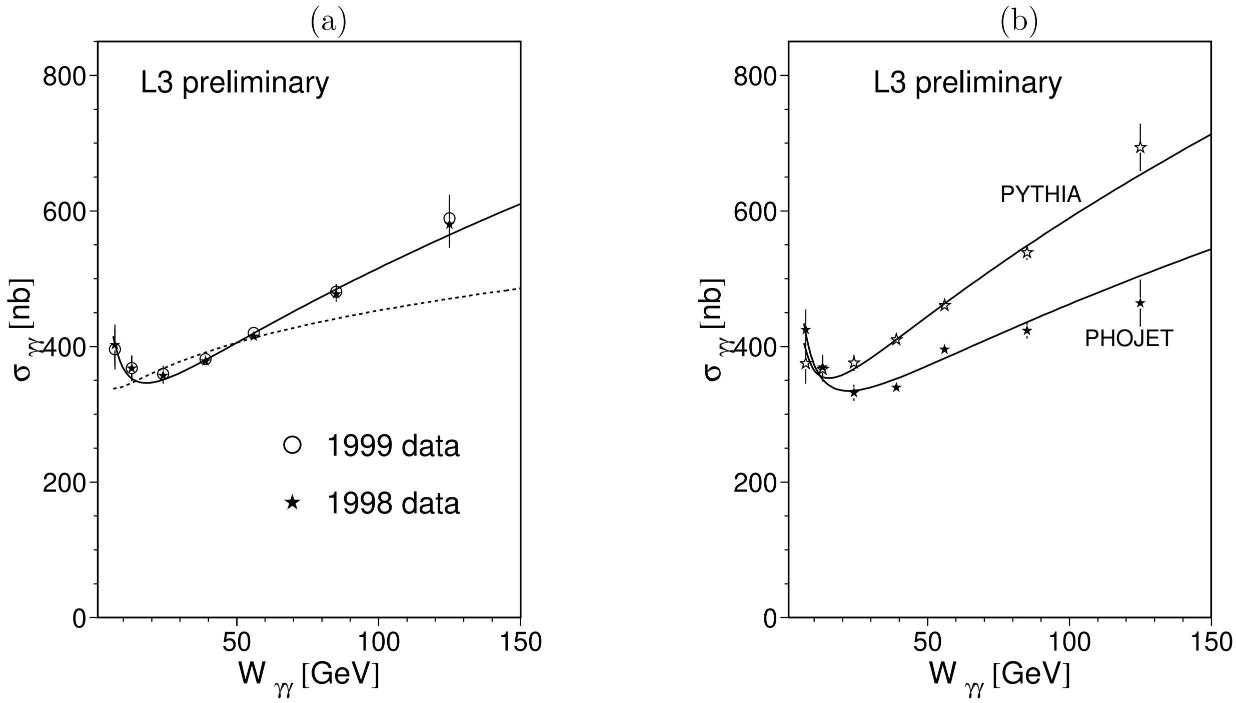

Figure 4: a) The data of 1998 at $\sqrt{s}$= 189 GeV are compared to the data of 1999 at $\sqrt{s}$= $192-202$ GeV. b) The two-photon total cross section obtained by correcting the full data sample with PHOJET (stars) and with PYTHIA (open points). The Regge fits described in the text (Table 3) are superimposed to the data. The continous lines are fits with the coefficient ϵ left as a free parameter, the dashed line is the fit with ϵ fixed to 0.095.

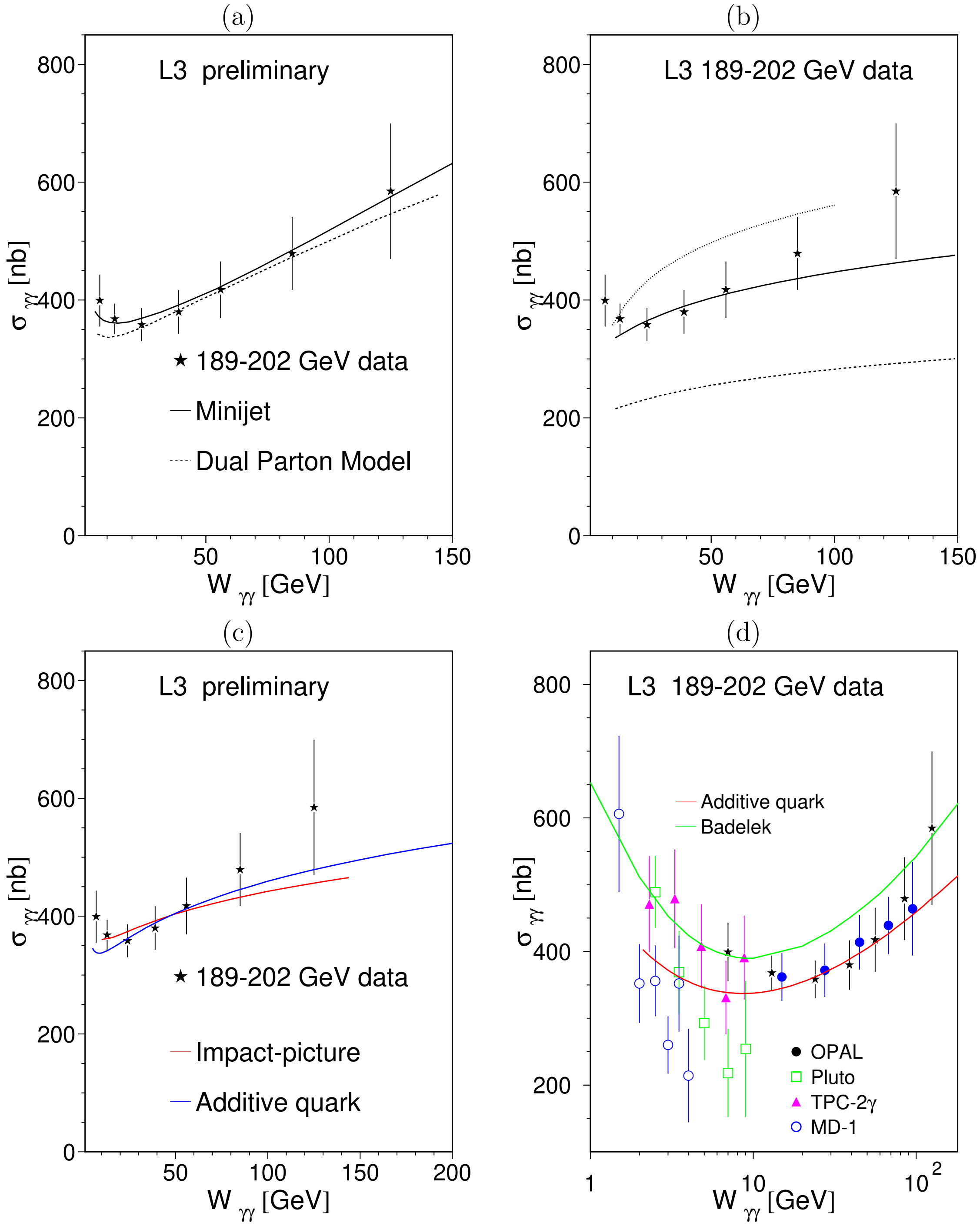

Figure 5: The two-photon total cross section compared to various model. a)Predictions of the minijet model [22] and of the Dual Parton Model [5] b) The calculation of G. Schuler and T. Sjöstrand [24] for the best estimation (full line), for the VDM contibution (dashed line) and for a maximum QCD contribution (dotted line). c) Predictions of the Additive Quark Model [28] and the Impact Picture model [29] d) The predictions of the Additive Quark Model [28] and of [27] are compared to all two-photon total cross section data. The statistical and full systematic errors are added in quadrature